NUMERICAL SIMULATION AND MODELLING OF HIGH-LIFT AERODYNAMICS IN GROUND EFFECT

Marcus BARTH*, Benoît CALMELS*, Bertrand AUPOIX**
***Airbus Operations SAS, ****ONERA/DMAE**

Keywords: *high-lift aerodynamics, ground effect, CFD, turbulence modelling, aerodynamic modelling*

Abstract

This paper presents the development of a simulation strategy for the numerical simulation and modelling of high-lift aerodynamics in ground effect. The objective is to improve the prediction accuracy of the ground effect using CFD.

The simulation strategy is defined and validated on a free-air test-case of a generic transport aircraft in landing configuration. In a first step, a mesh study is performed to alleviate mesh dependency. In a second step, different turbulence models are compared in order to evaluate their applicability to high-lift flows. In particular, two standard linear eddy viscosity models (LEVM) are compared to an Explicit Algebraic Reynolds-Stress Model (EARSM). The CFD solutions are examined in detail and validated against available data from wind tunnel tests. It is shown that the introduction of vortical flow corrections to the LEVMs significantly improves the reproduction of the local flow physics, as well as the prediction of global aerodynamic coefficients. Similar improvements have been obtained when using the EARSM model.

The developed simulation strategy is then applied to the ground effect. The influence of the ground effect on the local flow physics and on the global aerodynamic characteristics of the aircraft is studied in detail.

1 Introduction

The prediction of high-lift aerodynamics in ground effect plays an important role in the development of aircraft, both in the design (e.g. for the choice and the dimensioning of the high-lift devices), and in the prediction of the aerodynamic characteristics of the aircraft (i.e. the prediction of performance, handling qualities and structural stress of the aircraft). This work focuses exclusively on the latter aspect, i.e. the prediction of the aerodynamic behaviour of the aircraft in ground effect.

Currently, data production for high-lift aerodynamics is essentially done using wind tunnel testing (WTT) and flight testing (FT). WTT has the advantages of being a domain where airframe makers have a large experience and of providing data of appreciable quality. On the other hand, WTT provides data at relatively high costs and large time-scales and with some technical limitations in the range of applicability (e.g. limited insight in the flow physics, and, more specifically for ground effect testing, complex supports, safety margins limiting the minimal height of the aircraft over ground, belts to simulate the aircraft movement relative to the ground, etc.). The objective of this work is to define a feasible simulation strategy using modern CFD methods that allow to predict the aerodynamic behaviour of an aircraft in ground effect.

2 Test-Case

As test case, a generic transport aircraft in landing configuration has been selected, with a large availability of data from wind tunnel testing for model validation. The CAD model consist of the fuselage, the wing in high-lift configuration (including slats and flaps fully deflected, the wing main element, the flap track fairings, and the wing tip fences), the engine

installation (including the engine in- and outlet boundary panels, strakes, etc.), and the horizontal and vertical tail planes. The landing gear is not modelled in this study.

The computations are carried out in a first step in free air for flight conditions (flight Reynolds and Mach numbers during approach/landing) and for three angles of attack: α/α_{max}=0.25, 0.6 and 0.9. In a second step, computations are performed for the aircraft in the presence of ground for heights of *Dh/b*=0, 0.04 and 0.20 (where *Dh* is the height of the centre of gravity with respect to the aircraft on ground and *b* is the span of the aircraft). The slope of the aircraft is assumed to be equal to zero degrees (horizontal flight) for all computations. The engines are assumed to operate at maximum take-off (MTO) conditions.

3 CFD Models

The different physical and numerical models used in this study are described below, insisting on the different turbulence models used. The basic ideas and assumptions that are made during their derivation are recalled, as well as their strengths and weaknesses. This is to serve as theoretical basis for the discussion of the numerical results in chapter 4.

3.1 Mesh

For the mesh generation, the commercial software CENTAUR® is used. All meshes are unstructured and are generated using prism elements in the boundary layers and tetrahedron elements in the outer regions. A modular meshing approach is employed: The aircraft without horizontal tail plane (HTP), the HTP, and the farfield (including the ground panel) are contained in three separate modules that can be modified and meshed independently from one another. This is to allow for fast adaptation of the mesh to different heights and pitch angles for the ground effect study and to assure iso-mesh around the aircraft. All longitudinal test cases are computed on half-span meshes, whereas unsymmetrical computations (such as sideslip) are performed on full-span meshes.

3.2 Solver

As flow solver, the TAU code is used. This code has been developed by the DLR and is based on a finite-volume approach. As governing equations, the fully compressible mass-weighted averaged Navier-Stokes equations are solved on an unstructured grid. Boundary layers are treated with a low-Reynolds approach. For the spatial discretization, a cell-vertex approach with a dual metric is used. The inviscid fluxes are discretized using a second-order central differencing scheme with scalar dissipation, while the convective fluxes of the turbulence equations are discretized using a first-order central scheme for Spalart-Allmaras type turbulence models and a first-order upwind scheme for the Menter SST and the EARSM model. Time integration is performed with local time stepping using an implicit backward Euler scheme solved with the LUSGS linear solver. Multigrid cycling is used to accelerate convergence.

3.3 Turbulence Models

3.3.1 Linear Eddy-Viscosity Models

The linear eddy viscosity models (LEVM) are based on the Boussinesq-hypothesis, relating the Reynolds-stress tensor to the mean velocity field gradients by

$$-\overline{\rho u_i'' u_j''} = 2\mu_t \left(S_{ij} - \frac{1}{3}\frac{\partial u_k}{\partial x_k}\delta_{ij} \right) - \frac{2}{3}\bar{\rho} k \delta_{ij} \quad (1)$$

where μ_t is the eddy viscosity.

Spalart-Allmaras type turbulence models

The Spalart-Allmaras type turbulence models solve a single transport equation for the eddy viscosity $\nu_t = \mu_t/\rho$ in (1). The term in (1) containing the turbulent kinetic energy k is neglected, i.e. $k = 0$. The original version of the Spalart-Allmaras model (SAO) is proposed by Spalart and Allmaras in Ref. [1]. In Ref. [2], Edwards proposes a slightly different version of the Spalart-Allmaras original version, which modifies the modelled near wall behaviour, avoiding negative values of the strain-rate norm.

However, Spalart-Allmaras type models suffer from well-known deficiencies in flows

experiencing streamline curvature or flow field rotation (e.g. in vortex dominated flows). As shown in Refs. [4] and [5], standard turbulence models based on the Boussinesq-hypothesis significantly overpredict turbulence production in regions experiencing flow field rotation, leading to excessively high eddy viscosity levels in the vortex core and finally to an increased dissipation, spreading, or smearing of the vortex. Note that, physically, the flow should be laminar inside the vortex core, as shown in Ref. [6]. Several authors have proposed vortical flow corrections in order to remedy this problem (cf. e.g. Refs. [4], [5]). The FLOWer vortical flow correction introduces a rotation function to the production term of the turbulence transport equation of Spalart-Allmaras type turbulence models. This rotation function leaves the production term unchanged where the strain rate is larger than the vorticity, and decreases the turbulent production where vorticity dominates the strain (e.g. in vortex cores). The more general SARC model proposed by Spalart and Shur in Ref. [4] introduces a second term to the rotation function, which is activated in regions with streamline curvature or system rotation.

The Spalart-Allmaras type of turbulence models is selected in the NASA model performance evaluation due to their numerical behaviour and their prediction accuracy (cf. Ref. [3]). For this study, the Edwards' version of the Spalart-Allmaras model (SAE) and the SAE model with the FLOWer vortical flow correction (SAE+FLOWer) are selected for the turbulence model study.

Menter-SST models

In the case of two-equation k-ω models, the eddy viscosity in (1) is calculated from $\mu_t=\rho \cdot k/\omega$, where the turbulent kinetic energy k and the specific dissipation rate ω are solutions of two transport equations. The Menter baseline model (BSL) has originally been proposed in Ref. [7]. The Menter SST (Shear Stress Transport) model, equally introduced in Ref. [7], is a further improvement of the Menter BSL model. This model introduces a shear-stress correction to the definition of the eddy viscosity μ_t and changed coefficients in the inner layer.

However, the Menter k-ω models suffer from the same deficiencies as the Spalart-Allmaras type models in flows with flow field rotation. In Ref. [5], Kok introduces a correction to the production term in the ω-transport equation, where the strain rate is replaced by the rotation rate when the latter is bigger, hence increasing the turbulent dissipation in regions with large flow rotation. The production term in the k-equation remains unchanged.

The Menter SST is selected in the NASA model performance evaluation as the best overall model (cf. Ref. [3]). For this study, the Menter-SST model (SST) and the Menter-SST model with Kok's vortical flow correction (SST+Kok) are selected for comparison. The Kato-Launder modification proposed in Ref. [8] is applied to both models in order to avoid excessive turbulence production close to stagnation points. The authors would like to acknowledge that analysis posterior to this study have evidenced that the implementation of the Kok vortical flow correction in the used TAU version does not correspond to the formulation proposed by Kok in Ref. [5]; the conclusions drawn here may therefore be affected.

3.3.2 Explicit Algebraic Reynolds-Stress Models

In this class of turbulence models, the (linear) Boussinesq eddy-viscosity approximation is abandoned and the Reynolds-stress tensor is determined from a more general Explicit Algebraic Reynolds Stress Model (EARSM). This stress-strain relation can directly be derived from the Reynolds-Stress Transport Model; the remaining unknown terms are solutions of a two-equation background model. The EARSM-class models can therefore be considered as nonlinear two-equation models.

As EARSM-class models remain two-equation models, they are believed to offer the same advantages as standard k-ω models in terms of numerical stability and computational cost. Furthermore, by their construction, the EARSMs better reproduce complex flow phenomena, such as streamline curvature, rotation, or swirl and are therefore believed to have a wider range of applicability than the standard LEVMs (cf. Ref. [9]).

For this study, the Hellsten EARSM (*EARSM*) has been chosen (cf. Ref. [9]). This model uses the Wallin & Johansson EARSM as constitutive model, given by

$$-\overline{\rho u_i'' u_j''} = 2C_\mu^{eff} k\hat{S}_{ij} - \frac{2}{3}\rho k\delta_{ij} - \rho k a_{ij}^{ex} \quad (2)$$

where $\hat{S}_{ij}$ is the normalized mean strain tensor and a_{ij}^{ex} accounts for extra anisotropy. As background model, a modified version of Menter's BSL model is used.

3.4 Computation Strategy

In order to avoid hysteresis effects, CFD computations in free air are carried out by gradually increasing the angle of attack, starting from converged solutions in the linear range. Note that this strategy is currently not applicable in ground effect, as the aircraft attitude w.r.t. the ground-panel (i.e. the altitude *Dh* and the pitch angle θ) is fixed in advance by the mesh. For computations started from scratch, the engine in- and outlet boundary conditions are progressively increased from idle to maximum take-off in order to avoid numerical instability.

As convergence criterion, convergence of the density-residual and of the aerodynamic coefficients is used. The convergence criteria applied to the lift and to the pitching moment coefficients are 0.5 lift- and pitching-moment counts in the linear range and 1.0 lift- and pitching-moment counts in the non-linear range.

4 Definition and Validation of the Simulation Strategy in Free Air

The simulation strategy is developed and validated on the free-air test case and is then applied to the ground effect. The objective is to select appropriate physical and numerical models for the treatment of high-lift aerodynamics.

4.1. Physical Phenomena

The process of defining and validating the simulation strategy is based on a preliminary consideration of which flow phenomena are actually present in our flow field. This is to determine the question of *how much detail do we need*?

High-lift aerodynamics are characterized by a number of very general flow phenomena. These include (in no particular order): 1) transition and relaminarisation; 2) boundary layer and wake development in the presence of adverse pressure gradients; 3) confluent boundary layers; 4) vortex flows and streamline curvature; 5) complex flow detachment mechanisms; 6) large circulation around the lifting surfaces; 7) aero-elastic effects; as well as 8) multiple interactions between these phenomena. Note that experience shows that the presence of the ground does not add any additional physical phenomena to the flow, but changes their intensity and the interaction between each other.

It is apparent that the reliable prediction of the aerodynamic behaviour of an aircraft in ground effect will require accurate modelling of all relevant flow features mentioned above. This requires the intervention along the entire CFD chain, e.g. the generation of adequate meshes, the choice of appropriate physical and numerical models, and a post-treatment that allows to evidence and to verify the correct reproduction of the different flow phenomena involved. For simplicity, transition and aeroelastic effects will not be considered here.

4.2. Mesh Study

The objective of this mesh study is to build a mesh that *captures* all relevant flow features. Three half-span meshes with different refinement levels are studied: The coarse grid consists of $30{\cdot}10^6$ grid points ($80{\cdot}10^6$ elements), while the intermediate and fine grid contain $50{\cdot}10^6$ grid points ($130{\cdot}10^6$ elements) and $59{\cdot}10^6$ grid points ($148{\cdot}10^6$ elements), respectively, using local mesh refinement. All computations are performed with the Menter SST model. The different meshes are evaluated based on (a) a *microscopic* level (i.e. the resolution of all relevant flow features), and (b) on a *macroscopic* level (i.e. the global aerodynamic coefficients).

We will start with the *microscopic analysis* of the different flow features. The boundary layer

resolution is evaluated based on two criteria: The dimensionless wall distance (y^+) and the thickness of the boundary layer w.r.t. the thickness of the prism layer in the near-wall mesh. Analysis shows that initial estimations of the first cell height based on flat plate analogy lead to excessively high y^+ values around the leading edges of the wing. Local refinement of the first cell height largely improves the obtained y^+ values in these regions.

An aspect specific to high-lift configurations is the presence of confluent boundary layers, which form in the wake of the slats and of the wing main element. Velocity profiles in the wake of the slats are used to assess the mesh resolution (cf. Fig. 1). Analysis of the velocity profiles shows that the wake is dissipated too quickly for all meshes, despite a significant increase in the total number of mesh elements. It is concluded that the resolution of confluent boundary layers cannot be achieved by mesh refinement only. Potential ways of improvement currently under investigation in a separate study are to improve the interface between the tetrahedral and prism zones in this region, or the use of locally structured meshes.

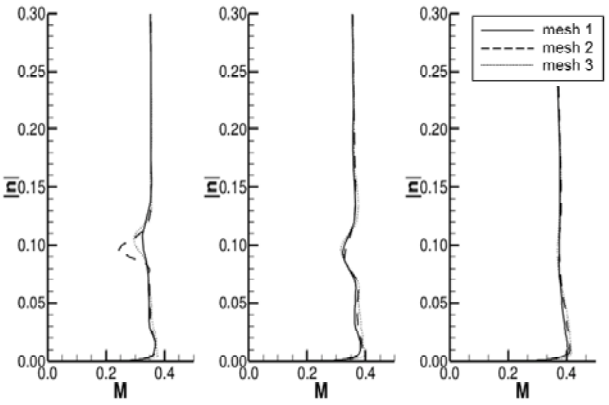

Fig. 1: Velocity profiles at $\Delta x/c$=8.8%, 9.2% and 10%, respectively, at α/α_{max}=0.6

A second aspect more or less specific to high-lift configurations is the need for high near field resolution: Aircraft in high-lift configuration generate large lift and circulation. As a consequence, sufficient near field resolution off the lifting surfaces is required in order to correctly capture the gradients present in these regions of the flow. The entropy increment indicator proposed in Ref. [10] is applied; Fig. 2 shows the contours of entropy around a three-element wing section. We see that the increase in entropy essentially rests confined within the boundary layers and wakes; the entropy increase outside of physical phenomena (e.g. linked to numerical dissipation) rests negligible.

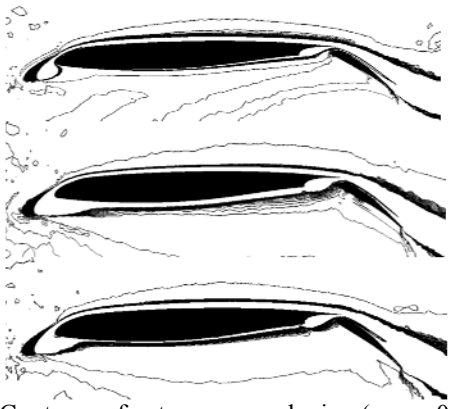

Fig. 2: Contours of entropy around wing (range 0~10^{-3}), coarse, intermediate, and fine mesh (α/α_{max}=0.25)

Another flow feature present in high-lift aerodynamics is vortex flows. It is important to note that, although the flow around a transport aircraft is not vortex-dominated, the presence of vortices has an important influence on the aerodynamic characteristics of the aircraft (e.g. on the flow detachment mechanisms through the strake vortices, or on the induced drag through the wing tip vortices). Here, the strake vortices will be discussed in some detail, due to their strong impact on the aerodynamic behaviour of the aircraft around stall. The quality of the mesh in view of the resolution of these vortical structures is essentially influenced by two parameters: The dimensions of the refined region and the level of mesh resolution. On the three meshes, different dimensions of the refined region and mesh resolutions have been applied. Fig. 3 shows the vorticity levels in the inner strake vortex for the three different meshes. One can clearly see that the inner strake vortex (*i*) is not satisfyingly resolved on the coarse mesh, whereas the intermediate and the fine mesh show a much better resolution of this vortex. Also, the position of vortex (*i*) is slightly shifted to the right on the coarse mesh, whereas the intermediate and the fine mesh show the vortex at the same location. The second vortex (*ii*), originating at the edge of the inner slat, is best captured on the fine mesh.

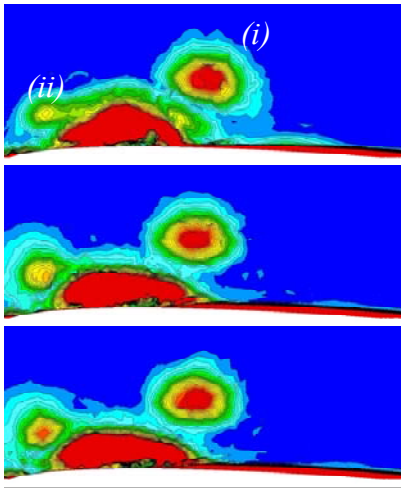

Fig. 3: Vorticity levels in the inner strake vortex, coarse, intermediate, and fine mesh (α/α_{max}=0.9)

On the *macroscopic* level, table 1 summarizes the aerodynamic coefficients obtained on the three meshes for α/α_{max}=0.6.

	mesh 1	mesh 2	mesh 3
$C_z/C_{z,max}$	0.6019	0.5985	0.6019
$C_x/C_{x,max}$	0.7856	0.7870	0.7905
$C_m/C_{m,max}$	0.9456	0.9413	0.9511

Tab. 1: Aerodynamic coefficients (α/α_{max}=0.6, aircraft without HTP)

Finally, the fine mesh (mesh 3) is retained.

4.3. Turbulence Model Study

After having determined *which* flow features are present within the flow field and having generated a mesh that *captures* all relevant flow features, the objective is now to choose a set of equations that is capable of correctly *reproducing* them. For this study, two standard LEVMs, i.e. the SAE and Menter SST models, are compared to the EARSM from Hellsten. The different turbulence models are evaluated based on their solution accuracy (i.e. their capacity to correctly reproduce both the local flow physics and the global aerodynamic coefficients), and their numerical performance.

4.3.1 Local flow physics

On a *microscopic* level, an important requirement towards a turbulence model is that it correctly reproduces the physics of the flow. Here, two flow features are discussed in detail: The strake vortices and the flow detachment mechanisms.

Fig. 4 shows the eddy viscosity levels for the different turbulence models in the strake vortex. For both the SAE and the SST models, the eddy viscosity is maximal in the core of the strake vortices. We recall that, physically, the vortex core should be laminar. In contrast, the same models *with* vortex correction (SAE+FLOWer and SST+Kok) and the EARSM model show low eddy viscosity levels inside the vortex cores (after the vortex roll-up), which is physically correct. Similar observations are made for the wing tip vortex and the slat cove flow.

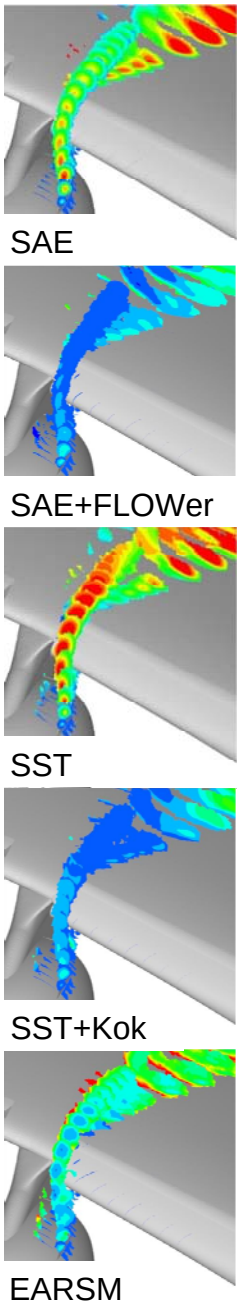

Fig. 4: Contours of μ_t (α/α_{max}=0.6)

Fig. 5: Flow detachment zones for SAE, SAE+FLOWer, SST, SST+Kok, and EARSM, at α/α_{max}=0.9

The second flow feature that we will look at is the flow detachment mechanism. In our case, the correct reproduction of the flow detachment is influenced by (a) the (general) ability of a given turbulence model to correctly predict flow detachment, and (b) the correct reproduction of the strake vortex, as it strongly interacts with the boundary layer on the wing suction side. This is a good example of how two different flow features interact. Fig. 5 shows the flow detachment zones at α/α_{max}=0.9.

When compared to results from WTT, the flow detachment zones predicted by the Spalart-Allmaras type and the EARSM models are (qualitatively) correct. The SST model, however, predicts separation too early. Some improvement is achieved by introducing the vortical flow correction to the SST model.

4.3.2 Global aerodynamic coefficients

On a *macroscopic* level, the obtained aerodynamic coefficients of the aircraft are used to access the prediction accuracy of the turbulence models.

In Fig. 6, the global aerodynamic coefficients obtained from CFD are compared to raw WTT data and WTT data scaled to flight.

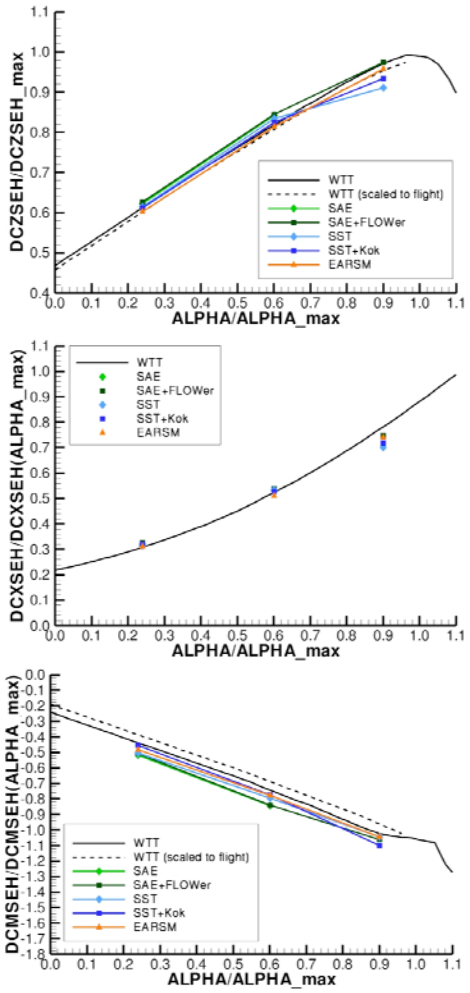

Fig. 6: Lift, drag, and pitching moment coefficients in function of alpha (A/C without HTP)

The EARSM clearly shows the best results. The Spalart-Allmaras type models show comparable results in terms of predicted drag and pitching moment, but are fairly off in the predicted lift. The SST and SST+Kok models show good results in the linear range, but predict separation too early. The introduction of the vortical flow correction helps to slightly improve the results obtained with the SST model.

4.3.3 Convergence

In terms of *numerical* performance, an important criterion in the selection of a turbulence model for industrial use is its ability to converge to steady state and its robustness. Convergence of the aerodynamic coefficients is important for the quality of the aerodynamic data, especially in view of the application to ground effect (being a relatively small effect), whereas robustness is required in order to use the model on an industrial scale and to compute the aircraft around its physical limits.

With regard to convergence to steady state and robustness, the Spalart-Allmaras type models show the best results, followed by the SST models. In the latter case, fluctuations in the convergence of the aerodynamic coefficients arise from premature flow detachment at large angles of attack. The EARSM yielded similar results as the other models for moderate angles of attack, but shows insufficient robustness for large angles of attack.

4.3.4 CPU time

A second criterion to assess the numerical performance of the different turbulence models is the computational time. Fig. 7 shows the CPU time per iteration and one million elements and the CPU time per computation (taking into account the number of iterations necessary to obtain convergence).

The differences in the CPU time per iteration are smaller than 25%. This difference essentially originates from the passage from the one-equation to the two-equation turbulence models (approx. 20%), while the introduction of a vortical flow correction or the use of the EARSM as constitutive model have little influence on the computational time per iteration (<5%). However, the differences in the computational time per CFD calculation are significant.

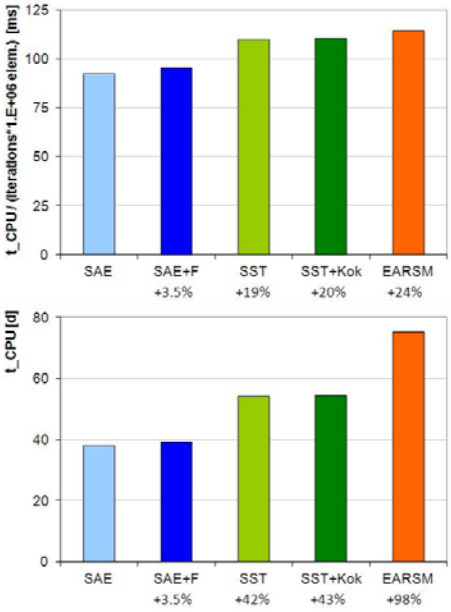

Fig. 7: Computational time per iteration (top) and per computation (bottom)

4.3.5 Conclusions

Table 2 summarizes the findings of this study in terms of the strengths and weaknesses of the different turbulence models studied.

	physics	aerodyn. coeff.	converg.	CPU time
SAE	−	○	++	++
SAE+F	++	○	++	++
SST	−−	−	+	+
SST+K	+	○	+	+
EARSM	++	++	−	○

Tab. 2: Comparison between turbulence models

With regard to *solution accuracy*, the SAE+FLOWer and the EARSM models have performed best. In particular, this study shows that, for the considered test case, the reproduction of the local flow physics and the prediction of the global aerodynamic coefficients can significantly be improved when standard LEVMs are extended with appropriate vortical flow corrections (i.e. SAE+FLOWer and SST+Kok). Similar improvements have been obtained with the EARSM from Hellsten.

In terms of *numerical performance*, the Spalart-Allmaras models were found to perform best, both with regard to stability and computational time, followed by the Menter SST model. The vortical flow corrections had no considerable

impact on stability or computational time. The EARSM model has shown some stability issues for higher angles of attack.

Finally, the SAE+FLOWer model is retained for the further study. However, although the SAE+FLOWer and the EARSM models show superior performance compared to the other models, there is still room for improvement, particularly in the high-end of the non-linear range and in the post-stall region. Current and future research will thus focus on improving the prediction accuracy in this field. As part of this research, the assessment of turbulence models will be continued and focus more specifically on the evaluation on higher order closure turbulence models, such as the Reynolds-Stress Transport Models.

5 Ground Effect Study

The simulation strategy developed in chapter 4 is now applied to study the ground effect. Computations are carried out at a number of representative flight points and validated against raw WTT data and WTT data scaled to flight. The CFD solutions are examined in terms of the impact of the ground effect on (a) the global aerodynamic characteristics of the aircraft or on isolated components (e.g. on the horizontal tail plane (HTP)), and (b) its impact on local flow features and on their interaction between each other.

5.1. Basic Longitudinal Test Case and VMU

The first application in ground effect is the basic longitudinal test case. Computations are performed from normal take-off conditions (at moderate angles of attack) up to the Velocity Minimum Unstick (VMU) manoeuvre (at very high angles of attack).

In Fig. 8, the obtained ground effect on the lift and the pitching-moment coefficients is compared to raw WTT data and WTT data scaled to flight. Note that the ground effect on lift is relatively small (around 5%), whereas the ground effect on the pitching moment is significant (approx. 70%). Comparison between the CFD results and the WTT data shows that the overall trends of the ground effect on lift are correctly reproduced by the CFD for moderate angles of attack. For larger angles of attack close to VMU conditions, however, the CFD results for lift suffer from premature flow detachment. For the ground effect on the pitching-moment, the CFD results fall between the raw and scaled WTT data, the CFD being in-line with the overall tendencies of the scaled WTT data.

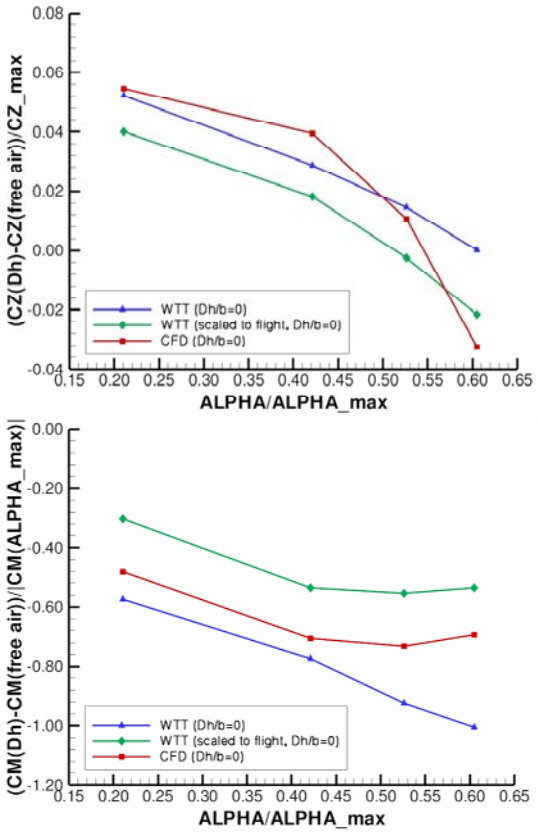

Fig. 8: Ground effect on lift and pitching moment coefficients at *Dh/b*=0 (aircraft without HTP)

The lift coefficient of the isolated HTP is shown in Fig. 9, as well as the ground effect on the HTP lift coefficient. It is interesting to note that the ground effect on the HTP lift coefficient is of the same order of magnitude as on the complete aircraft without HTP. As for the pitching moment, the HTP lift coefficient predicted by the CFD falls between the raw and the scaled WTT data. The overall tendencies predicted by CFD are again in-line with the scaled WTT data.

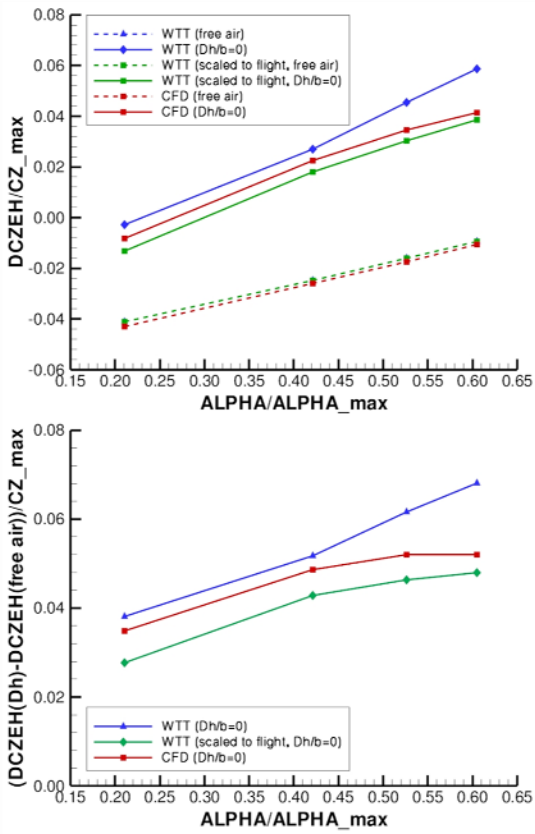

Fig. 9: HTP lift coefficient (top) and ground effect on HTP lift coefficient (bottom)

We will now look at what is happening in the HTP incident flow in terms of *local* flow phenomena. Fig. 10 shows the profiles of flow defection and dynamic pressure loss in the HTP incident flow obtained from the CFD solutions at different span-wise positions *y/B* (where *B* is the span of the HTP). The HTP leading edge is situated at *dZ=0*. From the downwash profiles, we can see that the downwash in free air is relatively large, whereas the downwash in ground effect takes much smaller values and finally reaches zero on the ground. This is a direct consequence of the flow deviation imposed by the ground. From the profiles of dynamic pressure, one can clearly see that in free air, both the wake of the wing and the jet pass beneath the HTP. In ground effect, however, the wake evidently impacts the HTP, while the jet rests confined on the ground and passes beneath. The ground effect thus influences both the downwash *and* the dynamic pressure in the incident flow of the HTP. This has to be taken into account when constructing aerodynamic models for the HTP lift and pitching-moment coefficients in ground effect.

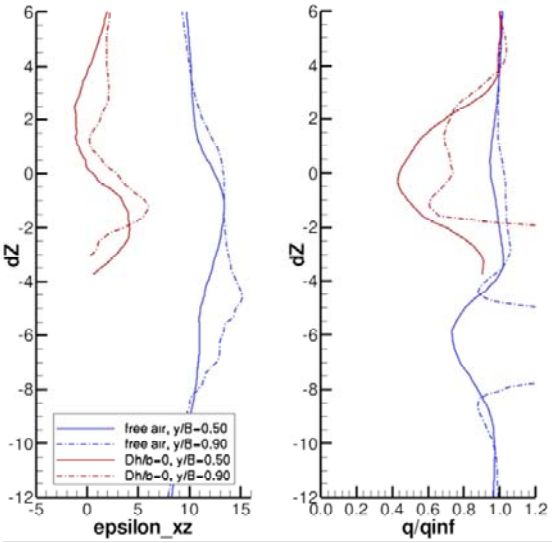

Fig. 10: Downwash and loss in dynamic pressure at 30% of the HTP cord length upstream of the HTP leading edge in free air and in ground effect (*Dh/b*=0); α/α_{max}=0.4

5.2. Parametric Studies

Parametric effects are studied in order to determine their impact on the aerodynamics of the aircraft in ground effect. Parametric effects include sideslip, roll angle, engine power settings, or crossed effects, such as sideslip with roll angle. It is important to note that for non-zero roll angles, the angle of incidence α and the angle of sideslip β become functions of θ, ψ, and φ. This has to be taken into account when considering crossed parametric effects (e.g. sideslip with roll angle) on meshes with iso-θ. Fig. 11 shows the ground effect on lift for longitudinal flight, sideslip, and sideslip with roll angle.

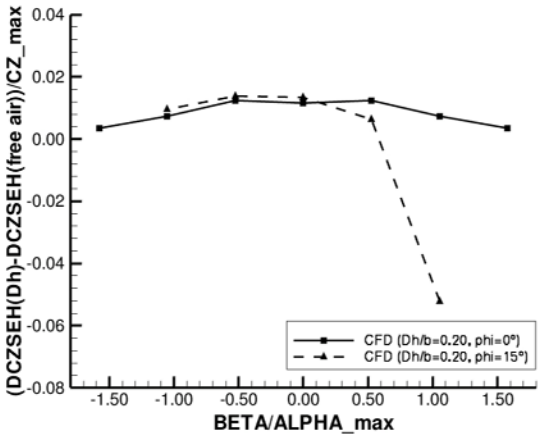

Fig. 11: Ground effect on lift coefficient (longitudinal flight, and sideslip with roll angle, θ/α_{max}=0.6)

From Fig. 11, we can see that flight with sideslip and roll angle cannot be considered as a combination of the sideslip and the roll effect. This is a consequence of the dissymmetry that arises from flight with sideslip and roll angle.

6 Conclusions

A simulation strategy has been developed and validated for the numerical simulation and modelling of high-lift aerodynamics in ground effect.

The simulation strategy has been defined on a free-air test case. In a first step, a mesh study has been performed to alleviate mesh dependency. In a second step, different turbulence models have been compared in order to assess their applicability to high-lift flows. In particular, two standard linear eddy viscosity models (LEVM), i.e. the Spalart-Allmaras and the Menter SST models, have been compared to the Explicit Algebraic Reynolds-Stress Model (EARSM) from Hellsten. The turbulence models have been evaluated in terms of solution accuracy and numerical performance. In terms of solution accuracy, it has been shown that the introduction of vortical flow corrections to the LEVMs significantly improves the reproduction of the local flow physics, as well as the prediction of global aerodynamic coefficients. Similar improvements have been obtained when using the EARSM model. The global aerodynamic coefficients obtained by CFD show good agreement with wind tunnel testing, especially in the linear and the beginning of the non-linear range. In terms of numerical performance, the Spalart-Allmaras type models have shown the best results. Finally, Edward's version of the Spalart-Allmaras model with FLOWer vortical flow correction has been selected.

The simulation strategy has then been applied to the ground effect. Parametric studies have been performed in order to determine the influence of sideslip, roll angle, engine power settings, or crossed effects, such as sideslip with roll angle, on the aerodynamics of the aircraft in ground effect. The obtained CFD solutions have been analyzed in view of the impact of the ground effect on the global aerodynamic characteristics of the aircraft and on the local flow physics. In terms of the (global) aerodynamic behaviour of the aircraft and of isolated aircraft components, the obtained CFD solutions have shown good agreement with available data from wind tunnel testing. In terms of the local flow physics, the incident flow to the horizontal tail plane has been analysed in detail. The obtained results contributed to our understanding of the ground effect on the horizontal tail plane and thus may help to improve aerodynamic modelling.

The developed simulation strategy allows to produce aerodynamic data within the prediction accuracy of prediction tools based on wind tunnel testing, while reducing data production time and costs. Additionally, CFD gives more insight in the flow physics of high-lift aerodynamics in ground effect.

7 Author's Coordinates

Marcus BARTH; Airbus Operations SAS; 316 route de Bayonne; 31060 Toulouse Cedex 09; FRANCE ; +33 (0)5 61 93 75 45 ; marcus.barth@airbus.com

References

[1] Spalart P.R. and Allmaras S.R., A one-equation turbulence model for aerodynamic flows. *30th Aerospace Sciences Meeting and Exhibit*, Reno, Nevada, AIAA 92-0439, 1992.

[2] Edwards J.R. and Chandra S., Comparison of eddy viscosity-transport turbulence models for three-dimensional, shock-separated flowfields. *25th Fluid Dynamics Conference*, Colorado Springs, Colorado, Vol. 34, No.4, 1993.

[3] Bardina J.E., Huang P.G. and Coakley, T.J., Turbulence modeling validation, testing, and development, *NASA TM 110446*, 1997.

[4] Spalart P.R. and Shur M., On the sensitization of turbulence models to rotation and curvature. *Aerospace Science and Technology*, Vol. 1, No. 5, pp 297-302, 1997.

[5] Dol H.S., Kok J.C. and Oskam B., Turbulence modelling for leading-edge vortex flows. *40th Aerospace Sciences Meeting & Exhibit*, Reno, Nevada, AIAA 02-14303, 2002.

[6] Bradshaw P., *Effects of streamline curvature on turbulent flow*, North Atlantic Treaty Organization, AGARD-AG-169, pp 57-61, 1973.

[7] Menter F.R., Improved two-equation k-ω turbulence models for aerodynamic flows. *NASA TM 103975*, 1992.
[8] Kato M. and Launder B.E., The modelling of turbulent flow around stationary and vibrating square cylinders. *9th Symposium on Turbulent Shear Flows*, Kyoto, 1993.
[9] Hellsten A. and Seppo L., Explicit algebraic Reynolds-stress modelling in decelerating and separating Flows, *AIAA Fluid Dynamics Conference*, Denver, Colorado, AIAA 2000-2313, 2000.
[10] Mitsuhiro M. and Kazuomi Y., Validation of flows on high-lift configurations by structured- and unstructured mesh method, *43th Aerospace Sciences Meeting and Exhibit*, Reno, Nevada, AIAA 2005.

Copyright Statement